Clinical Progress

Cell Stem Cell

Cardiac Repair in a Porcine Model of Acute Myocardial Infarction with Human Induced Pluripotent Stem Cell-Derived Cardiovascular Cells

Graphical Abstract

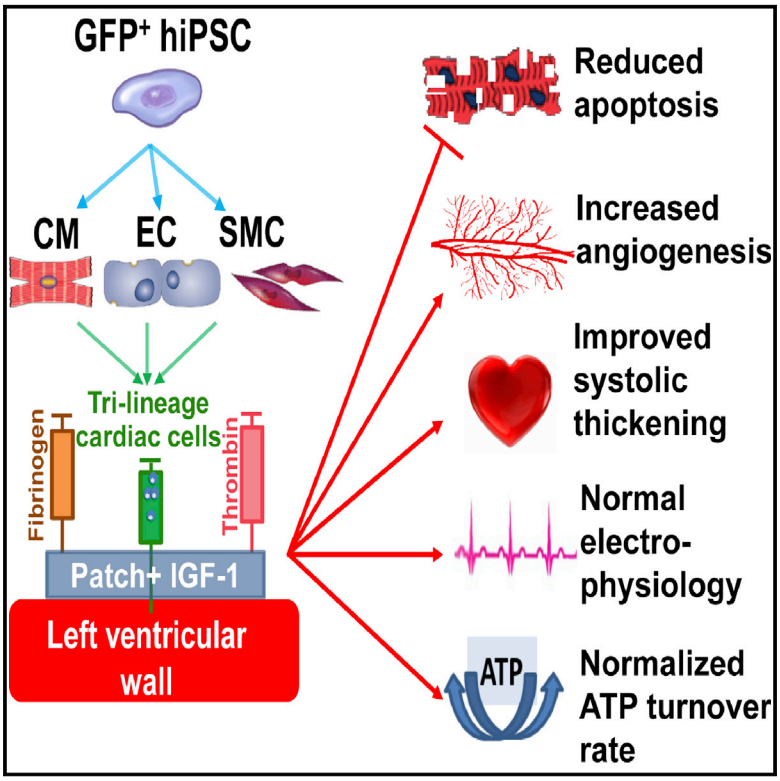

Highlights

Human iPSCs (hiPSCs) were differentiated into three cardiac lineages

hiPSC-derived cells were transplanted into a porcine model of myocardial infarction

Engraftment in combination with IGF-1-fibrin patch improves cardiac function

Intramyocardial delivery of hiPSC-cardiomyocytes did not cause arrhythmias

Authors

Lei Ye, Ying-Hua Chang, ..., Ying Ge, Jianyi Zhang

Correspondence

zhang047@umn.edu

In Brief

Large animal studies are required to assess the potential of human pluripotent stem cell (hPSC)-derived cells for cardiac repair. Ye et al. show that engraftment of hiPSC-derived cardiomyocytes, endothelial cells, and smooth muscle cells into a porcine model of myocardial infarction improves heart function and metabolism without inducing ventricular arrhythmias.

Ye et al., 2014, Cell Stem Cell 15, 750–761
December 4, 2014 ©2014 Elsevier Inc.
http://dx.doi.org/10.1016/j.stem.2014.11.009

CellPress

Cell Stem Cell
Clinical Progress

Cardiac Repair in a Porcine Model of Acute Myocardial Infarction with Human Induced Pluripotent Stem Cell-Derived Cardiovascular Cells

Lei Ye,[1,2] Ying-Hua Chang,[3] Qiang Xiong,[1] Pengyuan Zhang,[1] Liying Zhang,[1] Porur Somasundaram,[1] Mike Lepley,[2,4] Cory Swingen,[1] Liping Su,[1] Jacqueline S. Wendel,[5] Jing Guo,[1] Albert Jang,[6] Daniel Rosenbush,[1] Lucas Greder,[2] James R. Dutton,[2] Jianhua Zhang,[7] Timothy J. Kamp,[3,7] Dan S. Kaufman,[2,4] Ying Ge,[3,8] and Jianyi Zhang[1,2,5,6,*]
[1]Division of Cardiology, Department of Medicine
[2]Stem Cell Institute
University of Minnesota, Minneapolis, MN, 55455, USA
[3]Department of Cell and Regenerative Biology, University of Wisconsin, Madison, WI, 53705, USA
[4]Division of Hematology, Oncology, and Transplantation, Department of Medicine
[5]Department of Biomedical Engineering
[6]Department of Electrical and Computer Engineering
University of Minnesota, Minneapolis, MN, 55455, USA
[7]Department of Medicine, University of Wisconsin, Madison, WI, 53705, USA
[8]Department of Chemistry, University of Wisconsin, Madison, WI, 53706, USA
*Correspondence: zhang047@umn.edu
http://dx.doi.org/10.1016/j.stem.2014.11.009

SUMMARY

Human induced pluripotent stem cells (hiPSCs) hold promise for myocardial repair following injury, but preclinical studies in large animal models are required to determine optimal cell preparation and delivery strategies to maximize functional benefits and to evaluate safety. Here, we utilized a porcine model of acute myocardial infarction (MI) to investigate the functional impact of intramyocardial transplantation of hiPSC-derived cardiomyocytes, endothelial cells, and smooth muscle cells, in combination with a 3D fibrin patch loaded with insulin growth factor (IGF)-encapsulated microspheres. hiPSC-derived cardiomyocytes integrated into host myocardium and generated organized sarcomeric structures, and endothelial and smooth muscle cells contributed to host vasculature. Trilineage cell transplantation significantly improved left ventricular function, myocardial metabolism, and arteriole density, while reducing infarct size, ventricular wall stress, and apoptosis without inducing ventricular arrhythmias. These findings in a large animal MI model highlight the potential of utilizing hiPSC-derived cells for cardiac repair.

INTRODUCTION

Human induced pluripotent stem cells (hiPSCs) are promising therapeutic agents that can potentially generate an unlimited range and quantity of clinically relevant cell types that are not rejected by the patient's immune system. Several studies have reported generation of cardiomyocytes from hiPSCs (Burridge et al., 2012), and transplantation of these cells into rodent models of MI have suggested that they may provide functional benefit (Caspi et al., 2007; Laflamme et al., 2007; Shiba et al., 2012; van Laake et al., 2008). In a guinea pig model of cardiac injury, transplanted human embryonic stem cell-derived cardiomyocytes (hESC-CMs) showed electric coupling to native myocardium (Shiba et al., 2012). However, preclinical studies in large animal models of MI are necessary to fully evaluate the therapeutic potential of this approach and to empirically determine the optimal combination of cell types, supplementary factors, and delivery methods to maximize efficacy and stringently assess safety (Cibelli et al., 2013). To this end, Chong et al. utilized a nonhuman primate model of myocardial ischemia, injecting one billion hESC-CMs into the hearts of macaques with MI injury, and finding extensive evidence of engraftment, remuscularization, and electromechanical synchronization 2 to 7 weeks after transplantation (Chong et al., 2014). Despite these promising findings, telemetric electrocardiographic (ECG) evaluation demonstrated ventricular arrhythmias in some treated animals, suggesting further investigation of optimal cell quantities and delivery approaches is warranted.

Currently, poor engraftment of transplanted cardiomyocytes presents a significant barrier to transplantation-based approaches for myocardial cell therapy. In vitro studies strongly suggest that myocytes survive better when cocultured with endothelial cells (ECs) than when cultured alone (Xiong et al., 2012). Coadministration of ECs could enhance CM survival and benefit left ventricular (LV) myocardial perfusion, metabolism, and contractile activity through release of signaling molecules such as nitric oxide, vascular endothelial growth factor (VEGF), and insulin growth factor (IGF), which has also been shown to inhibit apoptosis (Davis et al., 2006; Brutsaert, 2003; Hsieh et al., 2006). Consistent with this hypothesis, we recently demonstrated that transplantation of hiPSC-derived ECs (hiPSC-ECs) and smooth muscle cells (hiPSC-SMCs) into ischemic porcine myocardial tissue contributes to

improvements in perfusion, wall stress, and cardiac performance (Xiong et al., 2012); however, myocardial repair and functional improvements may be even more extensive if primary force-producing myocardial cells are included in the population of transplanted cells.

In the present study, we injected three hiPSC-derived cell types (hiPSC-CMs, hiPSC-ECs, and hiPSC-SMCs) directly into injured hearts in a porcine large animal model of acute myocardial infarction. Cells were coinjected through an epicardial fibrin patch that provided prolonged release of the prosurvival factor insulin-like growth factor 1 (IGF-1), and cell engraftment and functional outcomes were evaluated. Our results show engraftment of cells from all three lineages at the site of injury, for at least 4 weeks after injection. This was accompanied by improvements in myocardial wall stress, metabolism, and contractile performance, and, importantly, did not lead to the development of ventricular arrhythmias. Together, these findings show that coadministration of multiple hiPSC-cardiovascular lineage cell populations promotes myocardial repair in large-animal models of MI.

RESULTS

Differentiation of hiPSCs into Cardiac-Lineage CMs, ECs, and SMCs

hiPSCs were reprogrammed from human dermal fibroblasts and engineered to express eGFP (Figure S1 available online) and differentiated into CMs via the Sandwich method (Zhang et al., 2012). Isolated areas of contracting cells typically appeared on day 7 of differentiation (Movies S1, S2, and S3) and were collected 1 week later for purification via a microdissection and preplating method. Expression of cardiac-specific proteins in differentiated hiPSC-CMs was evaluated on day 30 after cells started contracting. Nearly all hiPSC-CMs expressed slow myosin heavy chain, α-sarcomeric actin (Figure 1A), and the cardiac-specific myofilament cTnT (Figure 1B). Approximately 20%–30% of the hiPSC-CMs expressed the 2v isoform of myosin light chain (MLC2v) (Figure 1B, middle), which is found only in ventricular CMs, and cardiac connexin-43 was present at numerous points of contact between adjacent cells (Figure 1C). The purity of the final hiPSC-CM population was as high as 93% when evaluated via flow cytometry analysis of cTnT expression (Figures 1D and 1E) and >90% when evaluated via fluorescence immunostaining for cTnT expression (Figure 1F). hiPSC-ECs and hiPSC-SMCs were generated via established differentiation protocols (Hill et al., 2010; Woll et al., 2008) and expressed EC- and SMC-specific proteins (Figures 1G–1L).

hiPSC-Derived Cardiac Cells Engraft and Survive after Transplantation into a Porcine Model of Myocardial Infarction

We then tested our hypothesis that transplantation of three hiPSC-derived cardiac cell types would improve recovery after ischemic myocardial injury in a large-animal model (swine) of ischemia-reperfusion (IR) injury. A total of 92 pigs underwent the IR protocol; 89 pigs survived and were divided into five groups (Table S1). Animals receiving CMs, EC, and SMCs (Cell group) or CMs, ECs, SMC, and the fibrin/IGF-1 patch (Cell+Patch group) were injected with two million hiPSC-CMs, two million hiPSC-ECs, and two million hiPSC-SMCs (six million cells total) directly into the injured myocardium; for animals in the Cell+Patch group, the needle was inserted through an IGF-1-containing fibrin scaffold patch (Figure S2) that had been created over the site of injury. Animals in the Patch group were treated with scaffold patch alone, and both the patch and the cells were withheld from animals in the MI group. Animals in the Sham group underwent all surgical procedures for induction of IR injury, except for the ligation step, and recovered without any experimental treatments.

We then evaluated the engraftment and survival rates of the transplanted cells. Since the transplanted cells were genetically male and engineered to express GFP, while the recipient pigs were female, we performed quantitative PCR (qPCR) assessments for the human Y chromosome. Lineages of surviving cells were determined by staining for expression of the human-specific EC marker CD31 (hiPSC-ECs), for coexpression of GFP and α-smooth-muscle actin (SMA) (hiPSC-SMCs), and for coexpression of GFP and cTnT (hiPSC-CMs).

At 4 weeks after injury, 4.2% ± 1.1% of transplanted cells survived in animals in the Cells group while 8.97% ± 1.8% survived in the hearts of Cell+Patch animals. In contrast, 3.2% ± 0.4% of the two million cells administered to the CM group survived. Substantial proportions of all three transplanted cell types were observed in Cell+Patch hearts: 27.1% ± 5% of surviving transplanted cells were hiPSC-CMs, 34.2% ± 10% were hiPSC-ECs, and 40.5% ± 1% were hiPSC-SMCs. These observations suggest that the IGF-1-containing fibrin patch may have substantially improved the engraftment of all three hiPSC-derived cell lineages. Furthermore, GFP-expressing cells were present in cardiac muscle fibers (Figures 2A), but rarely in fibers composed of porcine cardiomyocytes (Figures S3A–S3D), suggesting that the transplanted hiPSC-CMs may have developed into new muscle fibers rather than incorporating into existing host cardiac muscle. GFP^+ cells were also identified in capillaries and arterioles (Figures 2B and 2C), although the proportion of vessels apparently generated directly from transplanted cells was less than 0.1%.

Transplantation of hiPSC-Derived Cardiac Cells Improves Cardiac Function and Bioenergetics after MI

Measurements of cardiac function were evaluated 1 and 4 weeks after injury and cell transplantation. Left-ventricular ejection fraction (LVEF) was significantly better in Cell+Patch group animals than in MI and Patch animals (Figure 3A) at 4 weeks. Systolic thickening fractions that reflect regional myocardial contractility were significantly greater in the infarct zone (IZ) and at the border zone (BZ) of the infarct in hearts from Cell+Patch animals than in MI hearts at both week 1 and week 4 time points (Figure 3B). Infarct size was significantly smaller in Cell+Patch hearts than in MI hearts ($p < 0.05$) at week 1, while the difference between Cell+Patch and Patch hearts approached statistical significance ($p = 0.051$) (Figure 3C). Measurements of regional wall stress performed 4 weeks after injury were significantly lower in Cell+Patch hearts than in Patch hearts (Figure 3D). Together, these results show that transplantation of multiple hiPSC-derived cardiac lineages, in combination with IGF-1/fibrin patch, improves cardiac function after MI.

We then determined whether these functional improvements in Cell+Patch animals were accompanied by improved

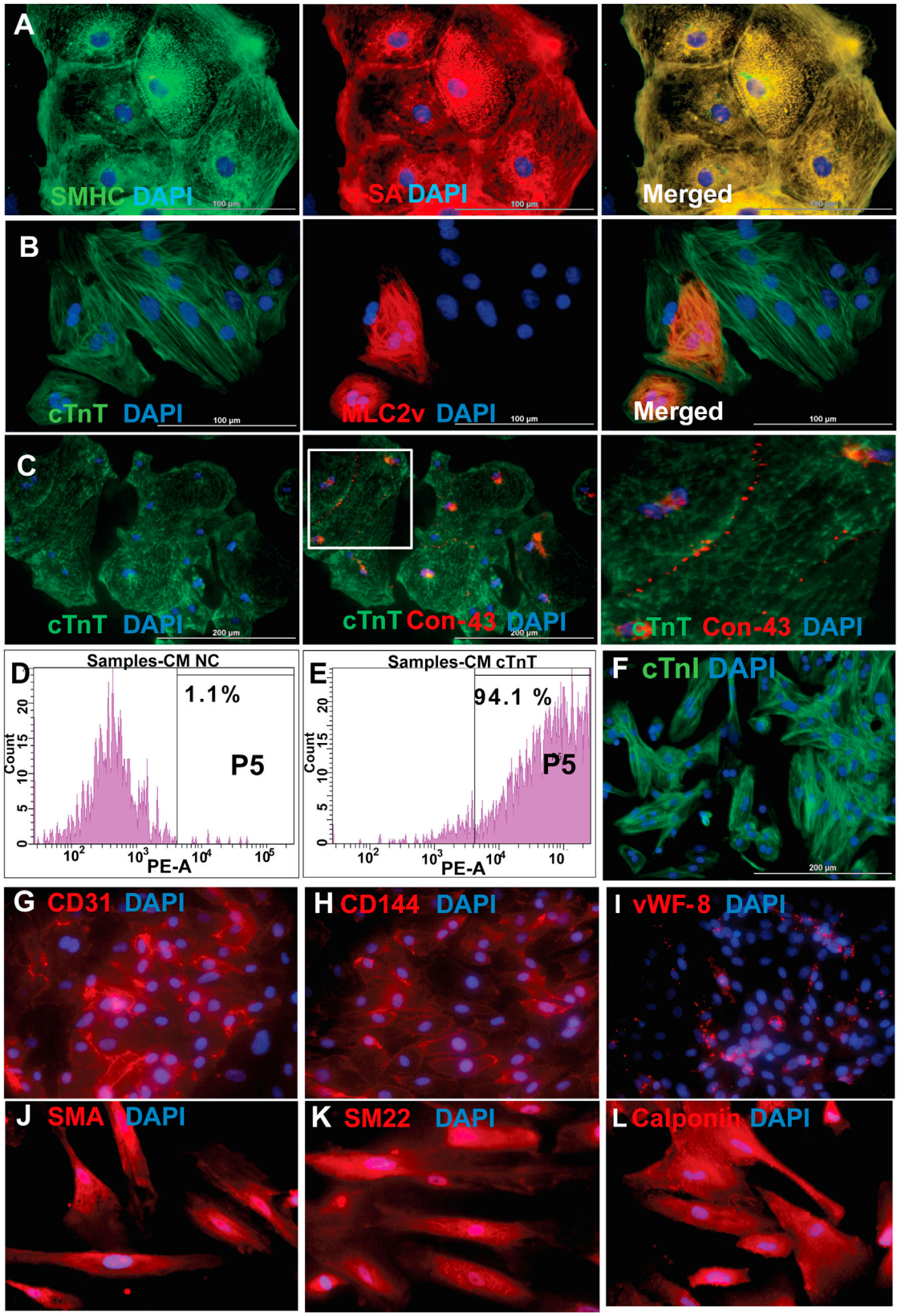

(legend on next page)

myocardial bioenergetics and efficient ATP utilization. Myocardial ATP hydrolysis rates were measured in vivo with the ^{31}P MRS-MST method (Xiong et al., 2013). Measurements were performed at the BZ of the infarct under both baseline and elevated cardiac work states in response to catecholamine stimulation. Myocardial PCr/ATP ratios that reflect mitochondrial energetic efficiency, were significantly higher in animals from the Cell+Patch group than in MI animals under baseline conditions (Figure 3E), while the rate of ATP hydrolysis was significantly higher in Cell+Patch group hearts than in MI and Patch hearts during high cardiac workload (Figure 3F); measurements in Patch and MI animals were similar under both conditions. Collectively, these observations indicate that the transplantation of hiPSC-derived cardiovascular cells improved LV pump function and myocardial energy metabolism while reducing infarct size.

Combined hiPSC-CM and Patch Treatment Does Not Induce Ventricular Arrhythmias

Arrhythmogenesis is a primary risk associated with pluripotent cell-derived CM therapy for treatment of cardiac disorders. In a recent study, significant ventricular arrhythmias were detected after transplantation of hESC-CMs in a nonhuman primate model of MI (Chong et al., 2014). Thus, we examined whether the hiPSC-CM patch transplantation protocol used here might be associated with onset of cardiac arrhythmia. Ischemia-reperfusion injury was induced in 16 pigs who then received the fibrin/IGF-1 patch alone (Patch group), the patch and ten million hiPSC-CMs (Patch+CMs), or neither experimental treatment (Table S1). ECGs were recorded continuously for 4 weeks afterward using an implantable loop recorder. Severe arrhythmias and ST elevations were observed in all animals during coronary artery occlusion and reperfusion, but no animal in any treatment group developed spontaneous arrhythmia during the 4-week follow-up period. Furthermore, no evidence of ventricular tachycardia (VT) or ventricular fibrillation (VF) was induced in response to programmed electrical stimulation (PES) in hearts of Patch+CM group animals, even when the most aggressive stimulation protocol was applied. Thus, the combined Patch+hiPSC-CM administration protocol used for the experiments described in this report does not appear to impair the electromechanical stability of swine hearts.

Transplantation of hiPSC-Derived Cardiac Cells Reduces Cardiomyocyte Apoptosis and Stimulates Nkx2.5 Expression after IR Injury

We next assessed how Cell+Patch treatment improves cardiac function. One possibility is through induction of cytoprotective mechanisms. To evaluate this possibility, we measured apoptosis in the hearts of animals sacrificed 3 days after IR injury and treatment (Figures 4A–4G). At the BZ of the infarct, apoptotic (i.e., TUNEL$^+$) cells were significantly less common in animals from the Cell+Patch group than in MI and Patch animals, both in the total cell population (Figure 4F) and specifically among CMs (i.e., cTnI$^+$ cells) (Figure 4G). Furthermore, the proportion of CMs that expressed Nkx2.5 (Figures 4H–4N), which has been shown to protect CMs from oxidative stress (Toko et al., 2002), was significantly greater in Cell+Patch animals than in MI animals at week 4 ($p < 0.05$), and the difference between Cell+Patch and Patch animals approached statistical significance ($p = 0.056$), at week 1 after IR injury (Figure 4N). Nkx2.5 expression in MI hearts increased at week 4 but remained significantly lower than in Cell+Patch hearts. Thus, transplantation of hiPSC-derived cells increased cell survival during the first few days after IR injury and is associated with upregulation of Nkx2.5 expression. The decline in apoptosis could also result from improvements in wall stress and decreased fibrosis. Consistently, examination of Masson-Trichrome-stained heart sections from animals sacrificed at week 4 showed thicker subepicardium in the region where the patch was applied (~2.44 mm) than in animals from the Sham (0.16 mm) or MI (0.88 mm) groups (Figure S4).

Transplantation of hiPSC-Derived Cardiac Cells Enhance the Vasculogenic Response to IR Injury

Increased angiogenesis could also contribute to improved ventricular function. We therefore assessed whether transplantation of hiPSC-derived cardiac cells promotes angiogenesis in peri-infarct border zone (BZ) of MI hearts. Four weeks after injury, CD31+vascular structures and arterioles that coexpressed CD31 and SMA were significantly greater in the BZ of Cell and Cell+Patch hearts than in the corresponding regions of MI and Patch hearts (Figure 5). Additionally, vascular density was significantly greater in the CM group than in the MI group. Thus, transplantation of the hiPSC-derived cardiac cells promoted neovascularization, probably by inducing paracrine mechanisms in recipient myocardial tissue (Table S2).

The cell and patch treatments may also have delayed the immune response to IR injury. While infiltration of cells expressing the inflammatory marker CD11b (Figures S5A–S5F) peaked 3 days after injury in the MI group, this was significantly delayed in the IZ and BZ regions of hearts from Cell+Patch animals (Figure S5G). CD11b$^+$ cells were significantly more common in Cell+Patch hearts than in MI hearts at week 1 but not at week 4, while the CM, Cells, and Patch groups showed a statistically nonsignificant

Figure 1. Differentiation of Human iPSCs into Cardiomyocytes, Endothelial Cells, and Smooth Muscle Cells

(A–C) hiPSCs were differentiated into CMs via the Sandwich method (Zhang et al., 2012), and the lineage of the differentiated hiPSC-CMs was confirmed via the expression of (A) slow myosin heavy chain (SMHC) and α-sarcomeric actin (α-SA); (B) cardiac troponin T (cTnT) and the ventricular- specific cardiomyocyte protein myosin light chain 2v (MLC2v); and (C) cTnT and the gap-junction protein connexin-43 (Con-43); nuclei were counterstained with DAPI. The boxed region in the second panel of (C) is shown at higher magnification.

(D–F) The purity of the hiPSC-CM population was evaluated via flow cytometry analysis of cTnT expression in (D) isotype controls and (E) purified hiPSC-CMs, and by (F) immunofluorescence analysis of cardiac troponin I (cTnI) expression; nuclei were counterstained with DAPI. Scale bar represents 100 μm in (A) and (B) and 200 μm in (C) and (F). (See also Movies S1, S2, and S3.) hiPSCs were differentiated into ECs and SMCs as described previously (Hill et al., 2010; Woll et al., 2008).

(G–L) The lineage of the differentiated hiPSC-ECs was confirmed via the expression of (G) CD31, (H) CD144, and (I) vWF-8; and (J–L) the lineage of the differentiated hiPSC-SMCs was confirmed via the expression of (J) smooth-muscle actin (SMA), (K) SM22, and (L) calponin. Nuclei were counterstained with DAPI. Magnification (G)–(L) = 200×. (See also Figure S1.)

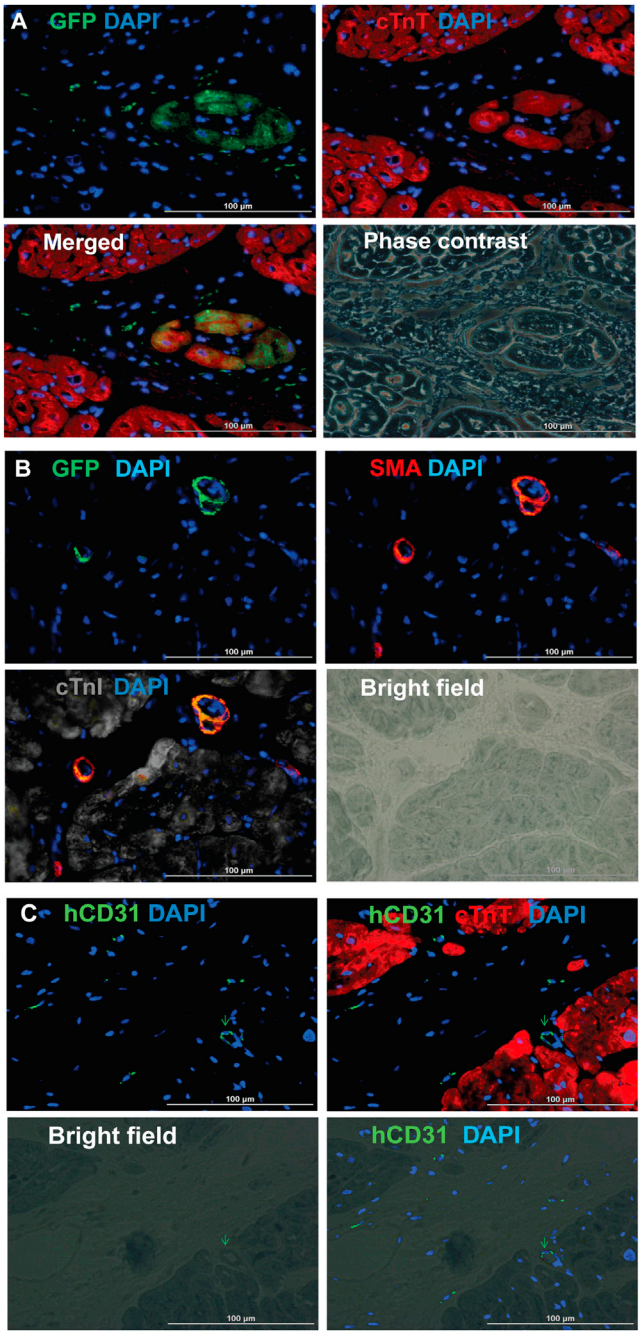

Figure 2. hiPSC-Derived Cardiac Cells Engraft and Survive after Transplantation into the Hearts of Swine with MI

(A) Engraftment of the injected cells was evaluated in sections stained for the presence of GFP; muscle fibers were visualized via fluorescent immunostaining for cTnT, and nuclei were counterstained with DAPI. The sections displayed in the first three panels were imaged with a phase-contrast microscope.

(B) Engrafted cells were identified in arterioles via immunofluorescent staining for the coexpression of GFP and SMA; muscle fibers were visualized via immunofluorescent staining for cTnI and nuclei were counterstained with DAPI.

(C) Engrafted cells were identified in blood vessels (i.e., capillaries and arterioles) via immunofluorescent staining for the human-specific isoform of CD31; muscle fibers were visualized via cTnT staining and nuclei were counterstained with DAPI. Scale bar represents 100 μm. (See also Figure S3.)

increase at weeks 1 and 4, suggesting a delayed host immune response following cell transplantation, possibly reducing immune rejection and increasing engraftment and survival of hiPSC-derived cells.

Paracrine Factor Release from the hiPSC-Derived Cells

This increase in angiogenesis observed after Cell+Patch treatment could be due to release of paracrine factors, as suggested by studies showing that endothelial cells promote cardiomyocyte survival (Xiong et al., 2012). To determine whether hiPSC-derived vascular cells possess cytoprotective effects similar to those previously reported in similar cell types, we cultured hiPSC-CMs under hypoxic conditions in media collected from the hiPSC-derived vascular cells (i.e., conditioned media) or with unconditioned (basal) media. hiPSC-CMs tended to shrink when cultured with unconditioned media but not when cultured with the conditioned media (Figures 5I and 5J). Culture in conditioned media was also associated with significant declines in hiPSC-CM apoptosis (Figures 5K, 5L, and 5N) and in the amount of cytoplasmic leakage of lactate dehydrogenase (LDH) from hiPSC-CMs (Figure 5M). Thus, hiPSC-derived vascular cells appear to release paracrine factors that protect hiPSC-CMs from hypoxic injury.

We then performed protein array analysis to identify paracrine factors that may be responsible for these in vitro cytoprotective effects and that might induce repair mechanisms in injured myocardial tissue. A total of 21 factors were detected, and their expression was confirmed in hiPSC-CMs, as well as hiPSC-derived vascular cells (Table S2). Several of the identified factors are known to impede apoptosis (angiogenin, angiopoietin, IL-6, MMP-1, PDGF-BB, TIMP-1, uPAR, and VEGF), induce cell migration or homing (angiogenin, angiopoietin, IL-8, MCP-1, MCP-3, MMP-9, uPAR, and VEGF), and promote cell division (angiogenin, angiopoietin, PDGF-BB, and VEGF), suggesting multiple paracrine mechanisms through which hiPSC-ECs and hiPSC-SMCs could promote CM survival and cardiac repair.

Myocardial Protein Expression after IR Injury and Cell Therapy

Understanding changes in the expression profile of myocardial proteins will help reveal the molecular mechanisms underlying improvements in left ventricular function associated with cell therapy. To provide further insights into these mechanisms, we performed a quantitative proteomics analysis on LV tissues from SHAM hearts and from MI hearts that were treated with or without hiPSC-derived vascular cells (which have both hiPSC-ECs and hiPSC-SMCs) after IR injury (Figure S6). We confidently identified 66 proteins whose expression pattern was altered in MI hearts but fully or partially restored to normal after cell transplantation (Figure 6). Thus, the functional benefits associated with cell therapy appear to be accompanied by a recovery of the myocardial protein expression profile of the recipient hearts.

DISCUSSION

The present study is among the first to evaluate the combined administration of three hiPSC-derived cardiovascular lineage cells in a large-animal model of ischemic myocardial injury. Our

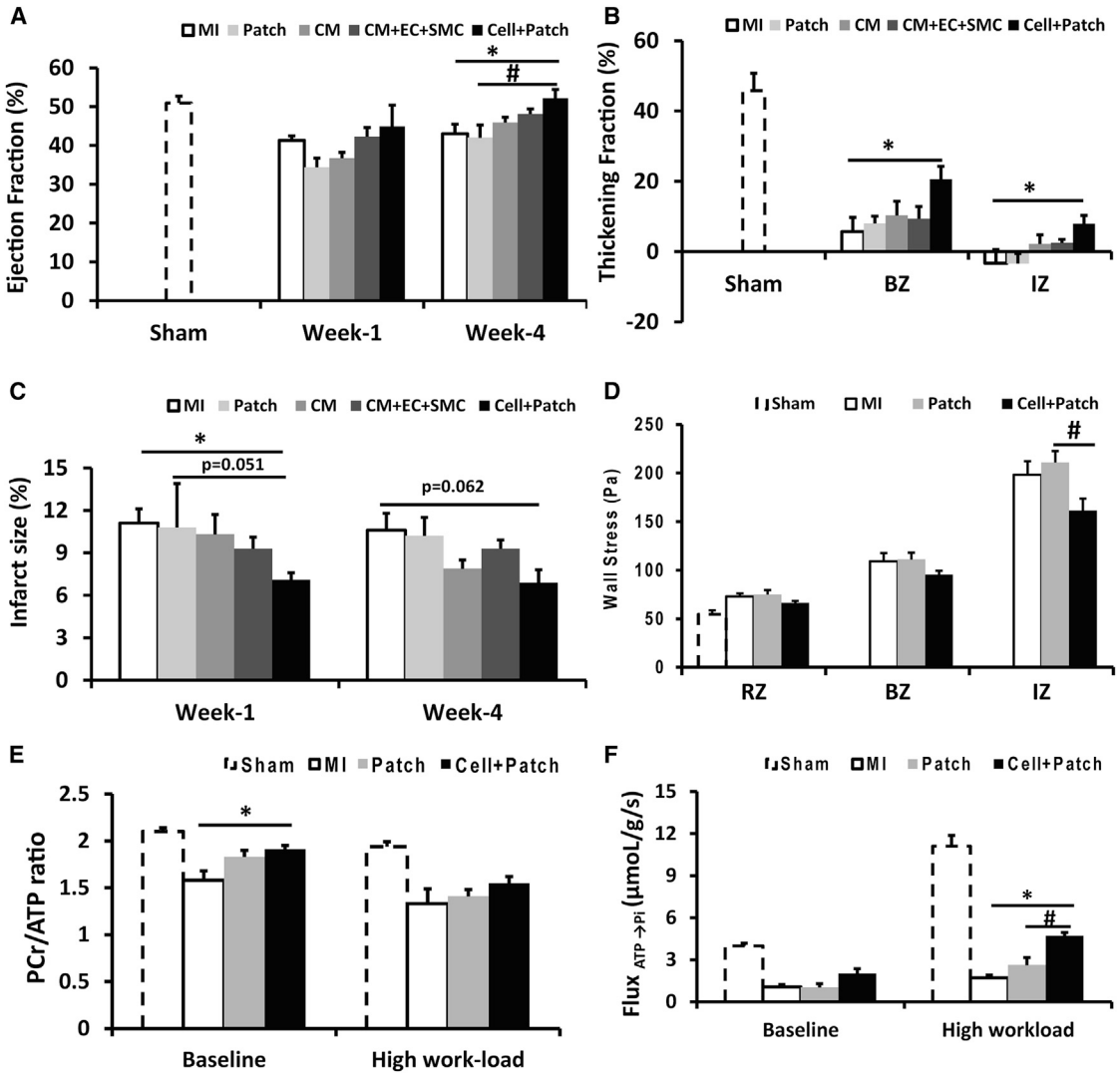

Figure 3. Transplanted hiPSC-Derived Cardiac Lineage Cells Improve Cardiac Function

(A) LV ejection fractions were evaluated at week 1 and week 4 after MI injury and treatment.

(B) LV wall systolic thickening fractions in the infarct zone (IZ) and at the border zone (BZ) of ischemia were evaluated at week 4.

(C) Infarct sizes were evaluated at week 1 and week 4 and expressed as a percentage of the LV surface area.

(D) LV wall stress in the IZ, in the BZ, and in uninjured regions of the myocardium (i.e., the remote zone [RZ]) was evaluated at week 4.

(E and F) Four weeks after MI injury and treatment, (E) PCr/ATP ratios and (F) the ATP hydrolysis rate were determined in the BZ under both baseline conditions and after a high cardiac workload was induced via catecholamine administration; measurements were obtained via a double-saturation ^{31}P MRS-MST protocol. For (B), (D), (E), and (F), measurements in Sham animals were performed in regions that corresponded to the site of injury in the other experimental groups. Data are presented as mean ± SEM, *p < 0.05 versus MI; #p < 0.05 versus Patch. (See also Figures S2 and S4 and Table S1.)

results indicate that when hiPSC-CM, hiPSC-SMC, and hiPSC-EC injection is performed through a fibrin patch that has been created over the injection site and contains gelatin microspheres that release IGF-1 into the surrounding tissue, the engraftment rate of the transplanted cells can be as high as 8.97% ± 1.8% 4 weeks after transplantation, which is ~20-fold greater than the engraftment rate observed when adult swine progenitor cells were evaluated in the same animal model (Zeng et al., 2007). Our results also demonstrate that the transplanted cells developed into functioning CMs and vascular cells and that the combination of hiPSC-CM, hiPSC-EC, and hiPSC-SMC injection with patch application led to significant improvements in LV wall stress, infarct size, systolic thickening fraction, vascular density, and ATP turnover rate. These findings are consistent with the concept that the severity of LV functional decline and structural remodeling is proportional to scar size (Pfeffer and Braunwald, 1990) and that LV dilatation and hypertrophy are exacerbated as increases in systolic wall stress propagate from the IZ and BZ to the adjacent myocardium (Pfeffer and Braunwald, 1990).

Previous attempts to isolate hiPSC- or hESC-derived CMs have been only moderately successful. Xu et al. (2006) used a method based on Percoll separation and cardiac body formation

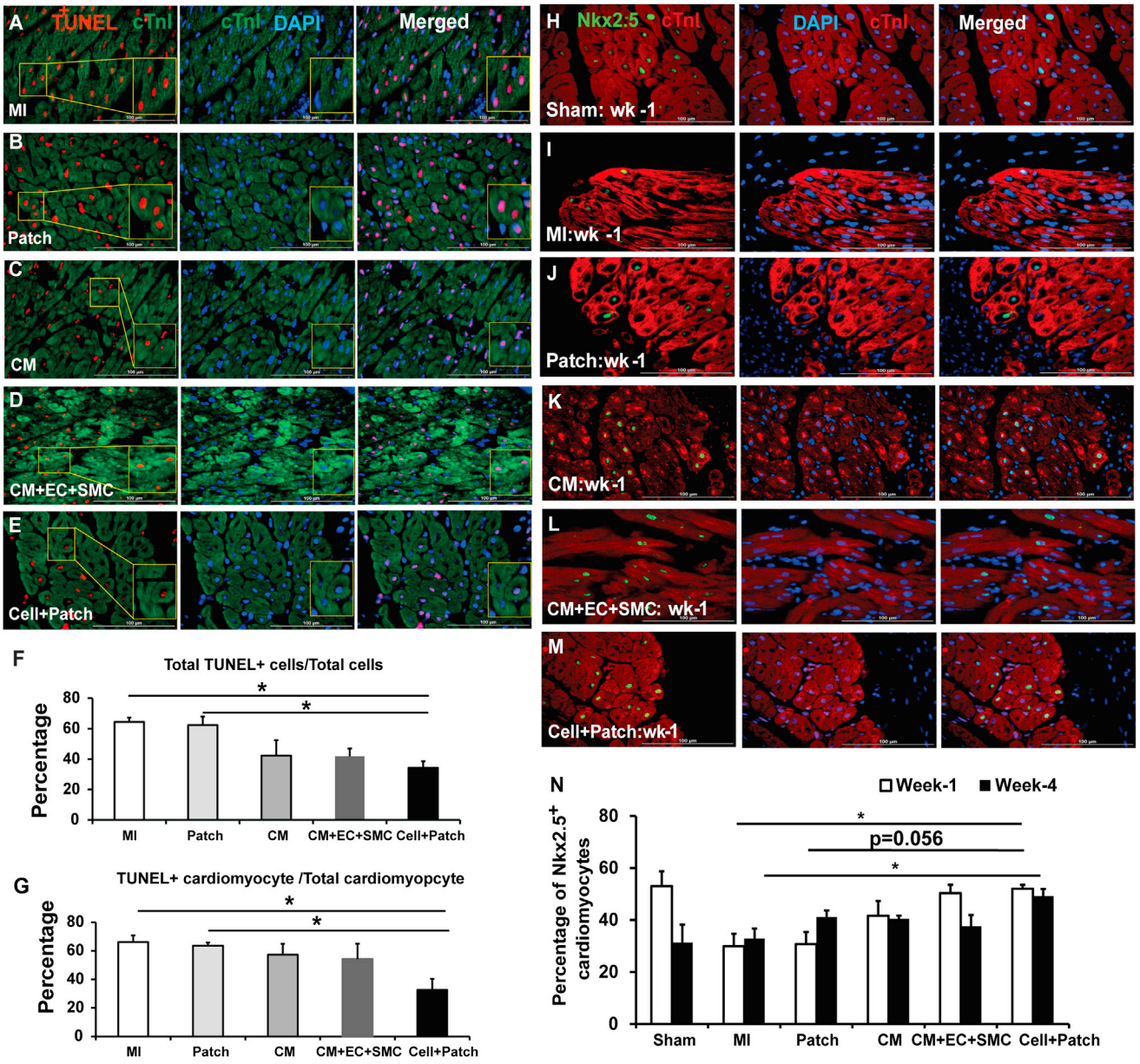

Figure 4. Transplantation of hiPSC-Derived Cardiac Cells Reduces Cardiomyocyte Apoptosis and Enhances Endogenous Cell Survival

(A–G) Apoptotic cells were identified in sections from the border zone of infarct in hearts from animals in the (A) MI, (B) Patch, (C) CM, (D) CM+EC+SMC, and (E) Cell+Patch groups with the TUNEL assay. Muscle fibers were visualized via fluorescent immunostaining for cTnI, and nuclei were counterstained with DAPI; the boxed regions toward the left of (A), (B), (C), (D), and (E) are displayed at higher magnification in the boxes at the right of the images. (F) Apoptosis was quantified as the percentage of cells that were positive for TUNEL staining. (G) Cardiomyocyte apoptosis was quantified as the percentage of cTnI-positive cells that were also positive for TUNEL staining.

(H–N) NkX2.5 expression was evaluated in sections from the border zone of infarct hearts that compared to Sham operated-normal hearts: (H) Sham, (I) MI, (J) Patch, (K) CM, (L) CM+EC+SMC, and (M) Cell+Patch. The immunofluorescent staining positives with anti-Nkx2.5 antibody are shown in green; muscle fibers were visualized via fluorescent immunostaining for cTnI, and nuclei were counterstained with DAPI. (N) The percentage of cardiomyocytes that expressed Nkx2.5 was determined at week 1 and week 4 after injury. Data are presented as mean ± SEM. *$p < 0.05$; scale bar represents 100 μm. (See also Table S2.)

to obtain hESC-CMs, but just 35%–66% of the isolated cells expressed slow myosin heavy chain or cTnT, suggesting that the purity of the obtained population would not be sufficient for use in large-animal models. With the differentiation protocol (Zhang et al., 2012) used here, 68% of the differentiated cells expressed cTnT, and the purity was subsequently increased to >90% via microdissection and preplating, yielding a total of three to four million hiPSC-CMs per well. This yield and purity is sufficient for experiments in large animal models and supports the feasibility of potential clinical trials.

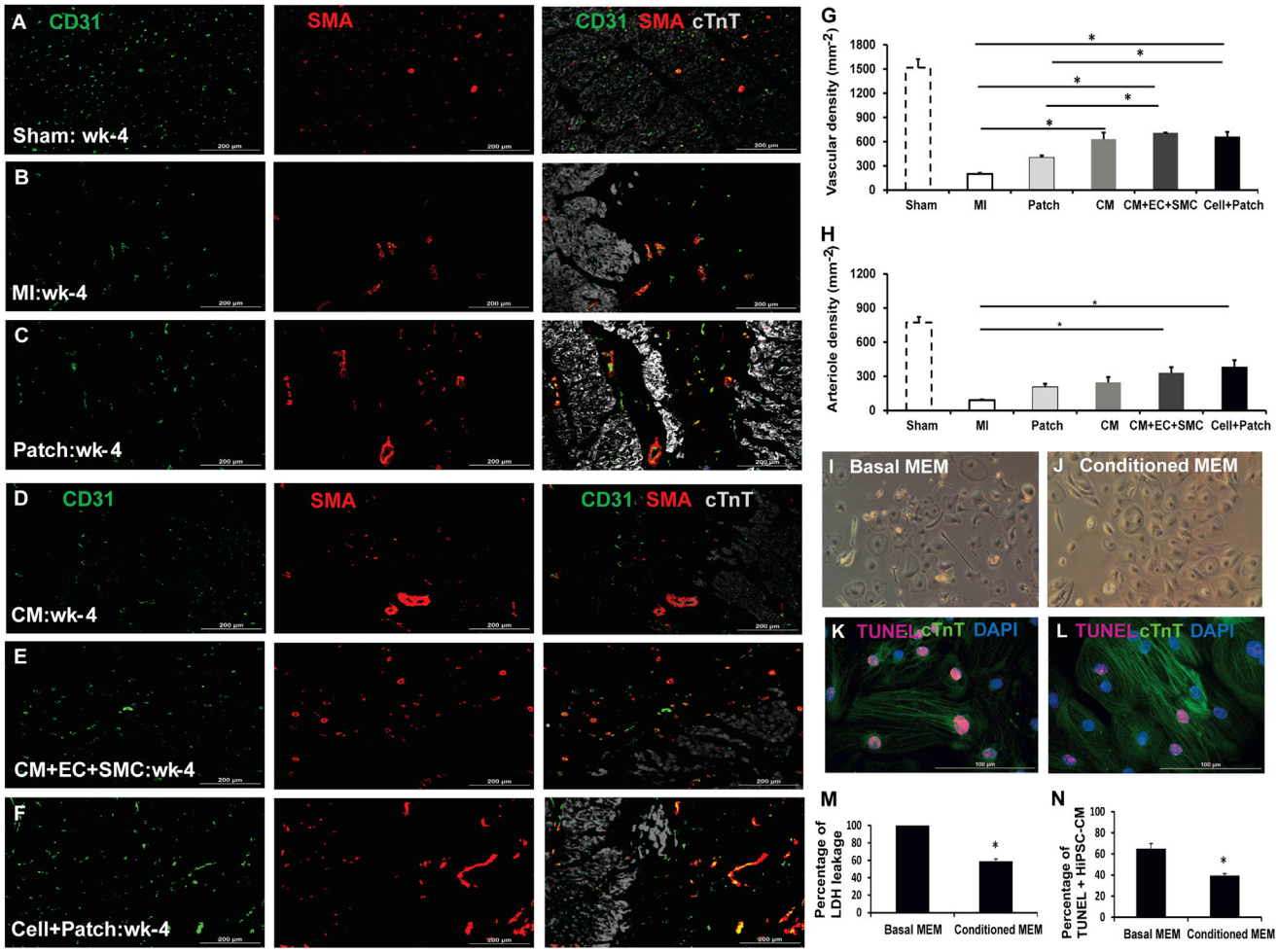

Figure 5. The hiPSC-Derived Cardiac Cells Enhance the Angiogenic Response and Inhibit Apoptosis

Vascular density and arteriole density at week 4 after MI were evaluated in sections from the border zone of infarct in the hearts of animals from the (A) Sham, (B) MI, (C) Patch, (D) CM, (E) CM+EC+SMC, and (F) Cell+Patch groups via immunofluorescent staining for CD31 and SMA; muscle fibers were visualized via cTnT staining. (G) Vascular density was determined by counting CD31+ vascular structures, and (H) arteriole density was determined by counting vascular structures that expressed both CD31 and SMA. *$p < 0.05$; scale bar represents 200 μm.

(I–N) hiPSC-CMs were cultured under hypoxic conditions in (I) basal media (Basal MEM) or (J) media collected from the hiPSC-derived vascular cells (Conditioned MEM) for 48 hr; then, (K and L) apoptotic cells were identified via the TUNEL assay, (M) cytotoxicity was quantified via the intensity of lactate dehydrogenase fluorescence observed in the media, and (N) apoptosis was quantified as the percentage of cells that were positive for TUNEL staining. *$p < 0.05$ versus basal MEM; magnification: 100× for (I) and (J); scale bar represents 100 μm. Data are presented as mean ± SEM. (See also Figure S5 and Table S2.)

One of the primary factors limiting the effectiveness of cell therapy is the low proportion of transplanted cells that survive in the recipient heart a few weeks after transplantation (Beauchamp et al., 1999; Qu et al., 1998; Tang et al., 2010; Zeng et al., 2007). Coadministration of a cytoprotective agent, such as IGF-1, can improve cell survival rate (Davis et al., 2006; Li et al., 1997; Wang et al., 1998), but the administered cells may still be lost after reestablishment of blood flow or be forced out of the myocardium along the needle track by high pressure during systolic contraction. Notably, a considerably higher rate of engraftment was observed in hearts from the Cell+Patch group, which was 2-fold greater than the rate observed in Cell group hearts, ~2.5-fold greater than observed in CMs hearts, and ~4-fold greater than when only hiPSC-derived ECs and SMCs were incorporated into a growth-factor-enriched patch (Shimizu et al., 2002; Xiong et al., 2013). This can be partially attributed to the fibrin patch itself, as the patch forms a physical barrier preventing ejection of the cells into the epicardial space while providing a prolonged IGF-1 supply to promote cell survival.

The overall engraftment rate for the three cell populations administered to Cell+Patch animals was ~9% and the proportion of cells that expressed EC-, SMC-, or CM-specific markers are ~34%, ~40%, and ~27%, respectively. Substantial engraftment of stem cell-derived CMs has also been observed in a primate model of postinfarction LV remodeling (Chong et al., 2014): ~2% of the LV was composed of engrafted cells, but the precise engraftment rate could not be calculated because the engrafted cells were not counted. However, macaque hearts are

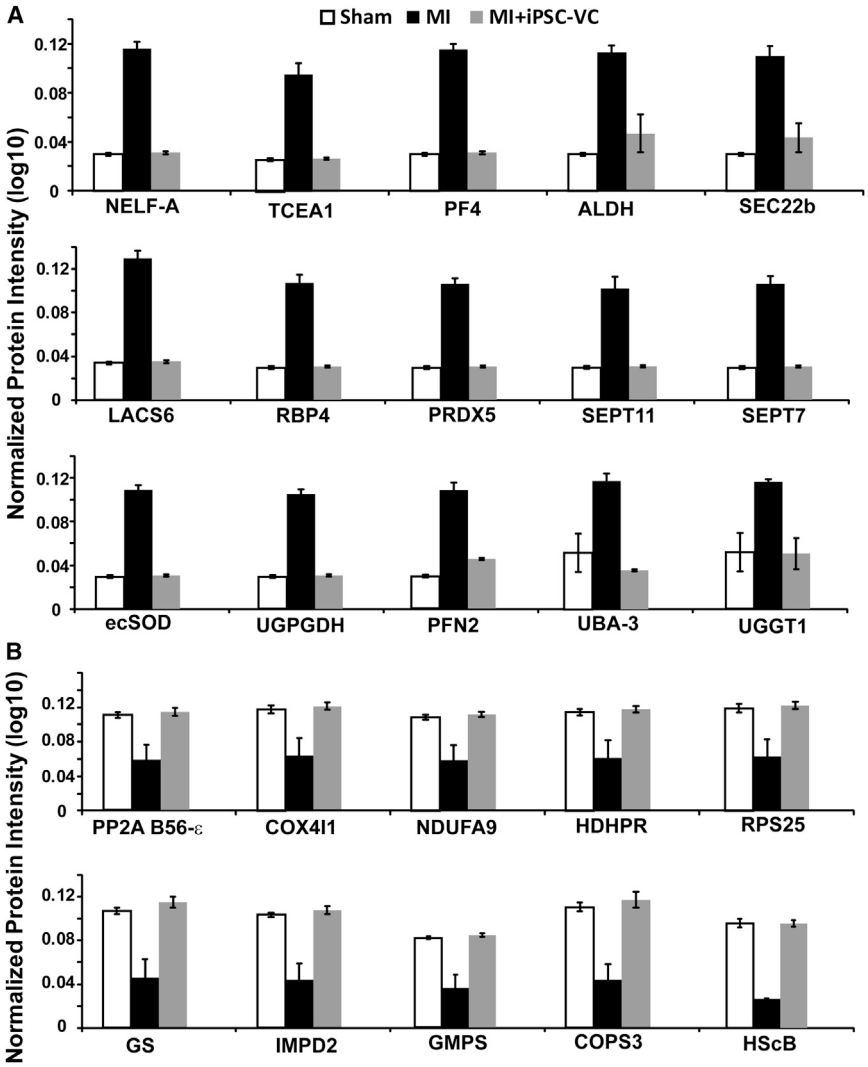

Figure 6. Protein Expression Levels Are Significantly Altered in MI and Partially Restored by Cell Transplantation

Myocardial protein expression profiles were evaluated in animals that had been treated with (MI+iPSC-VC) or without (MI) hiPSC-VC transplantation after experimentally induced MI; control assessments were performed in animals that underwent all surgical procedures for the induction of MI except for the ligation step (SHAM); results are displayed for 25 proteins whose expression levels (A) increased or (B) decreased after MI and were restored to normal levels by cell therapy. NELF-A, negative elongation factor A; TCEA1, transcription elongation factor A protein 1; PF4, platelet factor 4; ALDH, aldehyde dehydrogenase (mitochondrial); SEC22b, vesicle-trafficking protein SEC22b; LACS6, long-chain-fatty-acid-CoA ligase 6; RBP4, retinol-binding protein 4; PRDX5, peroxiredoxin-5 (mitochondrial); SEPT11, septin-11; SEPT7, septin-7; ecSOD, extracellular superoxide dismutase (Cu-Zn); UGPGDH, UDP-glucose-6-dehydrogenase; PFN2, profiling-2; UBA-3, NEDD8-activating enzyme E1 catalytic subunit; UGGT1, UDP-glucose:glycoprotein glucosyltransferase 1; PP2A B56-ε, serine/threonine-protein phosphatase 2A 56 kDa regulatory subunit ε isoform; COX4I1, cytochrome C oxidase subunit 4 isoform 1, mitochondrial; NDUFA9, NADH dehydrogenase (ubiquinone) 1 α subcomplex subunit 2; HDHPR, dihydropteridine reductase; RPS25, 40S ribosomal protein S25; GS, glutamine synthetase; IMPD2, inosine-5′-monophosphate dehydrogenase 2; GMPS, GMP synthase (glutamine-hydrolyzing); COPS3, COP9 sinalosome complex subunit 3; HScB, iron-sulfur cluster co-chaperone protein HScB (mitochondrial). Data are presented as mean ± SEM. (See also Figures S6 and S7.)

approximately one-sixth the size of human hearts (37–52 g versus ~300 g), which contain approximately three billion CMs, and ~70% of cardiac mass is contained in the LV; thus, the LVs of the animals used in the primate study probably contained ~350 million CMs, approximately seven million of which (i.e., 2% of 350 million) were the transplanted hESC-CMs. Since one billion hiPSC-CMs were administered to each macaque, the engraftment rate appears to have been ~0.7%, which is consistent with other rates reported in the literature (Zeng et al., 2007) and ~10-fold lower that the rate of hiPSC-CM engraftment observed in the Cell+Patch animals in the present study.

One of the most critical concerns associated with cardiac cell therapy is the development of arrhythmogenic complications. The study by Chong et al. (2014) illustrates that transplantation of human CMs to large animal post-MI models can unmask potential arrhythmic complications that are not observed in comparable small animal models (Shiba et al., 2012). All the monkeys studied by Chong et al. (2014) that received hESC-CMs developed spontaneous arrhythmia during the EKG follow-up evaluations. In the present study, we used a strategy of a smaller cell dose and aiming at mobilization of the endogenous cardiac progenitors, which we have reported earlier (Zeng et al., 2007; Xiong et al., 2013). We used a 100-fold lower dose of hiPSC-CMs compared to Chong's report and found no increase of spontaneous or PES-induced arrhythmia in any of the animals that received cell therapy. The remarkably better electrical stability achieved with our approach may be attributable, in part, to the smaller cell dose used (ten million versus one billion) and targeting the cytokine-associated mobilization of the endogenous progenitors (Xiong et al., 2013; Zeng et al., 2007). Electromechanical connectivity may be more extensive between native tissues and tissues generated through endogenous repair mechanisms than between native tissues and large piece of cardiac tissue that develop directly from the engrafted cells. Coadministration of ECs has been linked to the regulation of cardiovascular physiology (Brutsaert, 2003; Hsieh et al., 2006) and could have further improved myocardial recovery primarily through the enhancement of cytokine-associated mechanisms. These data also indicate that strategies designed to promote the paracrine effect of transplanted CMs and ECs maybe be more desirable in cardiac cell therapy.

Transplantation of hiPSC-derived cells was also associated with increases in the expression of Nkx2.5 in host cardiomyocytes,

which is known to protect cardiomyocytes from oxidative damage (Toko et al., 2002). Furthermore, myocardial perfusion is maintained by the regulatory activity of small resistant vessels (Frame and Sarelius, 1993), so the significant increase in myocardial arteriole density observed in the BZ of Cell+Patch-treated hearts also probably contributed to declines in apoptosis and to the preservation of contractile function. The increase in arteriole density appears to have occurred through the sprouting of preexisting microvessels in the BZ of the treated hearts, because nearly all of the vessels were GFP negative. The increase in arteriole density was also accompanied by a significant improvement in the myocardial ATP turnover rate (Figure 3F). The calculated rate, which incorporates the rates associated with all enzymatic processes that support contraction and relaxation as well as the rates generated by rapid near-equilibrium enzymes, was markedly reduced at the BZ of infarction in MI hearts, while measurements under high workload conditions were significantly greater in Cell+Patch animals than in animals from either the MI or Patch group.

Cyclosporine was administered to animals from all treatment groups to reduce the likelihood of immune rejection in animals treated with the hiPSC-derived cells. Nevertheless, assessments of $CD11b^+$ cell density suggest that the immune response was both elevated and delayed in Patch, CM, CM+EC+SMC, and Cell+Patch animals (though the increase was significant in only the Cell+Patch group). Both the patch and the transplanted cells could have contributed to this increase, because the patch was created by combining fibrin with thrombin, which is known to amplify the inflammation induced by ischemia (Chen and Dorling, 2009), and because the transplanted cells released inflammatory cytokines such as MCP-1 and IL-6. Notably, IL-6 production was 8-fold and 20-fold higher in hiPSC-ECs than in hiPSC-CMs or hiPSC-SMCs, respectively. Future study may be required to find an optimal dosage of cyclosporine or addition of other immunosuppression regimen, such as FK506, to minimize the immune rejection and achieve higher cell engraftment rate.

In conclusion, the studies described in this report evaluate the combined use of hiPSC-ECs, hiPSC-SMCs, and hiPSC-CMs in a porcine model of ischemia reperfusion myocardial injury. Our results demonstrate that when the enhanced cell delivery was achieved by an IGF-1-containing fibrin patch, the engraftment rate was remarkably greater than achieved with any other delivery method used in the porcine IR model (Zeng et al., 2007). Furthermore, the combination of all three cell types with extended, patch-mediated IGF-1 administration was associated with significant improvements in myocardial wall stress, apoptosis, arteriole density, metabolism, and contractile function. Collectively, these observations support the feasibility of future mechanistic studies of hiPSC-derived cardiac cells in large animal models. Studies with longer follow-up periods will also be needed to ensure that the benefits of treatment are maintained and to fully characterize any potential adverse effects that may be associated with this promising therapeutic modality.

EXPERIMENTAL PROCEDURES

Generation and Characterization of hiPSC-Derived Cardiac Cells

The hiPSC-CMs, hiPSC-SMCs, and hiPSC-ECs used in this study were generated from two hiPSC lines: DriPS16 (Cell+Patch group) and GRiPS (for the CM and CM+EC+SMC groups). Both hiPSC lines were reprogrammed from male, human, neonatal, dermal fibroblasts by transfecting cells with either lentivirus (DriPS16) or Sendai virus (GRiPS) coding for OCT4, SOX2, KLF4, and C-MYC and then engineered to constitutively express GFP. Cells were cultured in hiPSC growth medium with irradiated mouse embryonic fibroblasts and passaged every 6–7 days (Wilber et al., 2007).

hiPSCs were differentiated into ECs and SMCs as described previously (Hill et al., 2010; Woll et al., 2008). hiPSC-ECs were characterized via the expression of CD31, CD144, and vWF-8 (Xiong et al., 2012). hiPSC-SMCs were characterized via the expression of α-smooth muscle actin (SMA), SM22, and calponin.

In vitro cytoprotection assays are detailed in Supplemental Experimental Procedures

Paracrine Factor Release from Cultured hiPSC-CMs, ECs, and SMCs

hiPSC-CMs (3.5×10^5) and hiPSC-SMCs (3.5×10^5) were cultured in 6-well plates, washed three times with DPBS, and then cultured in 1 ml RPMI basal medium; hiPSC-ECs (4×10^5) were cultured in 1 ml EBM2 basal medium. The medium was collected 48 hr later and analyzed with the Human Angiogenesis Antibody Array G1 Array (RayBiotech). Measurements were corrected for background signals via control assessments with basal media that had been exposed to identical conditions.

Synthesis of IGF-containing microspheres and patch manufacture are detailed in Supplemental Experimental Procedures.

Porcine IR Injury Model and Treatment

Experiments were performed in female Yorkshire swine (~13 kg, 45 days of age, Manthei hog farm, Elk River, MN) (Xiong et al., 2012). The experimental protocol was approved by the IACUC of the University of Minnesota, and all experimental procedures were performed in accordance with the Animal Use Guidelines of the University of Minnesota and consistent with the National Institutes of Health *Guide for the Care and Use of Laboratory Animals* (NIH publication No 85-23).

A total of 108 pigs underwent the ischemia reperfusion (IR) protocol (Table S1). Ninety-two pigs were used in the first part of the study: two pigs died of ventricular fibrillation during occlusion, and one died of cardiac arrhythmia 1 week after IR injury while the MRI data were being collected. The remaining 89 pigs were divided into six groups. Animals in the CM+EC+SMC and Cell+Patch groups were treated by injecting two million hiPSC-CMs, two million hiPSC-ECs, and two million hiPSC-SMCs (six million cells total) directly into the injured myocardium; for animals in the Cell+Patch group, the needle was inserted through an IGF-1-containing fibrin patch that had been created over the site of injury. Animals in the Patch group were treated with the patch alone, and both the patch and the cells were withheld from animals in the MI group. Animals in the SHAM group underwent all surgical procedures for the induction of IR injury except for the ligation step and recovered without any of the experimental treatments. Sixteen pigs were used in loop recorder study. The Patch+CM group used in the arrhythmogenesis experiments exposed to a protocol of fibrin patch enhanced delivery of ten million hiPSC-CMs on surface of the injured myocardium (Table S1).

Patch application was performed by suspending 5 mg of microspheres (loaded with 2.5 μg IGF-1) in 1 ml fibrinogen solution (25 mg/ml); then, the fibrinogen solution was coinjected with 1 ml thrombin solution (80 NIH units/ml, supplemented with 2 μl 400 mM $CaCl_2$ and 200 mM Ɛ-aminocaproic acid) into a 2.3-cm-diameter plastic ring that had been placed on the epicardium of the infarcted region to serve as a mold for the patch; the mixture usually solidified within 30 s (Xiong et al., 2012). Cells were suspended in 1 ml MEM and administered via ten intramyocardial injections (0.1 ml/injection).

Cardiac MRI and MR Spectroscopy are detailed in Supplemental Experimental Procedures

The ECG Monitoring and Programmed Electrostimulation Physiology Studies

The implantable loop recorders (Medtronic-Reveal) were placed in the left paraspinal area inferior to the angle of the scapula in the subcutaneous plane. It was sutured in the place where the best electrograms were obtained and there was no evidence of myopotential noise. It was programmed in the conventional manner to document VT and asystole. The loop recorder was

interrogated at the time of explantation when the animals were sacrificed 4 weeks after the cell therapy.

The programmed electrostimulation physiology studies (PES study) were done at the time of sacrifice in 4 weeks. The PES study was done from the epicardium in an open-chest fashion. The PES study was done from two sites: one close to the infarct and one remote from the infarct. The study was done with a Medtronic screw lead in the epicardium and the Bard system was used for stimulation. It was done at two cycle lengths at 400 ms and 300 ms drive trains. Four additional stimuli were given till effective refractory period (ERP) was reached or 160 ms.

hiPSC-EC, hiPSC-SMC, and hiPSC-CM engraftment rate and immunohistochemical evaluations are detailed in Supplemental Experimental Procedures.

Experimental Procedures for proteomics are detailed in Supplemental Experimental Procedures.

Statistical Analysis

Results are presented as mean ± SEM. Comparisons among groups were analyzed for significance with one-way ANOVA. A value of $p < 0.05$ was considered significant. Results identified as significant via ANOVA were reanalyzed with the Tukey correction. Statistical analyses were performed with SPSS software (version 20).

SUPPLEMENTAL INFORMATION

Supplemental Information includes Supplemental Experimental Procedures, six figures, two tables, and three movies and can be found with this article online at http://dx.doi.org/10.1016/j.stem.2014.11.009.

ACKNOWLEDGMENTS

The authors would like to thank W. Kevin Meisner, Ph.D., E.L.S., for his editorial assistance. This work was supported by US Public Health Service grants NIH RO1s, HL UO1 100407, HL UO1 099773, and P41RR08079.

Received: April 21, 2013
Revised: March 24, 2014
Accepted: November 12, 2014
Published: December 4, 2014

REFERENCES

Beauchamp, J.R., Morgan, J.E., Pagel, C.N., and Partridge, T.A. (1999). Dynamics of myoblast transplantation reveal a discrete minority of precursors with stem cell-like properties as the myogenic source. J. Cell Biol. *144*, 1113–1122.

Brutsaert, D.L. (2003). Cardiac endothelial-myocardial signaling: its role in cardiac growth, contractile performance, and rhythmicity. Physiol. Rev. *83*, 59–115.

Burridge, P.W., Keller, G., Gold, J.D., and Wu, J.C. (2012). Production of de novo cardiomyocytes: human pluripotent stem cell differentiation and direct reprogramming. Cell Stem Cell *10*, 16–28.

Caspi, O., Huber, I., Kehat, I., Habib, M., Arbel, G., Gepstein, A., Yankelson, L., Aronson, D., Beyar, R., and Gepstein, L. (2007). Transplantation of human embryonic stem cell-derived cardiomyocytes improves myocardial performance in infarcted rat hearts. J. Am. Coll. Cardiol. *50*, 1884–1893.

Chen, D., and Dorling, A. (2009). Critical roles for thrombin in acute and chronic inflammation. J. Thromb. Haemost. *7* (1), 122–126.

Chong, J.J., Yang, X., Don, C.W., Minami, E., Liu, Y.W., Weyers, J.J., Mahoney, W.M., Van Biber, B., Cook, S.M., Palpant, N.J., et al. (2014). Human embryonic-stem-cell-derived cardiomyocytes regenerate non-human primate hearts. Nature *510*, 273–277.

Cibelli, J., Emborg, M.E., Prockop, D.J., Roberts, M., Schatten, G., Rao, M., Harding, J., and Mirochnitchenko, O. (2013). Strategies for improving animal models for regenerative medicine. Cell Stem Cell *12*, 271–274.

Davis, M.E., Hsieh, P.C., Takahashi, T., Song, Q., Zhang, S., Kamm, R.D., Grodzinsky, A.J., Anversa, P., and Lee, R.T. (2006). Local myocardial insulin-like growth factor 1 (IGF-1) delivery with biotinylated peptide nanofibers improves cell therapy for myocardial infarction. Proc. Natl. Acad. Sci. USA *103*, 8155–8160.

Frame, M.D., and Sarelius, I.H. (1993). Regulation of capillary perfusion by small arterioles is spatially organized. Circ. Res. *73*, 155–163.

Hill, K.L., Obrtlikova, P., Alvarez, D.F., King, J.A., Keirstead, S.A., Allred, J.R., and Kaufman, D.S. (2010). Human embryonic stem cell-derived vascular progenitor cells capable of endothelial and smooth muscle cell function. Exp. Hematol. *38*, 246–257, e1.

Hsieh, P.C., Davis, M.E., Lisowski, L.K., and Lee, R.T. (2006). Endothelial-cardiomyocyte interactions in cardiac development and repair. Annu. Rev. Physiol. *68*, 51–66.

Laflamme, M.A., Chen, K.Y., Naumova, A.V., Muskheli, V., Fugate, J.A., Dupras, S.K., Reinecke, H., Xu, C., Hassanipour, M., Police, S., et al. (2007). Cardiomyocytes derived from human embryonic stem cells in pro-survival factors enhance function of infarcted rat hearts. Nat. Biotechnol. *25*, 1015–1024.

Li, Q., Li, B., Wang, X., Leri, A., Jana, K.P., Liu, Y., Kajstura, J., Baserga, R., and Anversa, P. (1997). Overexpression of insulin-like growth factor-1 in mice protects from myocyte death after infarction, attenuating ventricular dilation, wall stress, and cardiac hypertrophy. J. Clin. Invest. *100*, 1991–1999.

Pfeffer, M.A., and Braunwald, E. (1990). Ventricular remodeling after myocardial infarction. Experimental observations and clinical implications. Circulation *81*, 1161–1172.

Qu, Z., Balkir, L., van Deutekom, J.C., Robbins, P.D., Pruchnic, R., and Huard, J. (1998). Development of approaches to improve cell survival in myoblast transfer therapy. J. Cell Biol. *142*, 1257–1267.

Shiba, Y., Fernandes, S., Zhu, W.Z., Filice, D., Muskheli, V., Kim, J., Palpant, N.J., Gantz, J., Moyes, K.W., Reinecke, H., et al. (2012). Human ES-cell-derived cardiomyocytes electrically couple and suppress arrhythmias in injured hearts. Nature *489*, 322–325.

Shimizu, T., Yamato, M., Isoi, Y., Akutsu, T., Setomaru, T., Abe, K., Kikuchi, A., Umezu, M., and Okano, T. (2002). Fabrication of pulsatile cardiac tissue grafts using a novel 3-dimensional cell sheet manipulation technique and temperature-responsive cell culture surfaces. Circ. Res. *90*, e40.

Tang, X.L., Rokosh, G., Sanganalmath, S.K., Yuan, F., Sato, H., Mu, J., Dai, S., Li, C., Chen, N., Peng, Y., et al. (2010). Intracoronary administration of cardiac progenitor cells alleviates left ventricular dysfunction in rats with a 30-day-old infarction. Circulation *121*, 293–305.

Toko, H., Zhu, W., Takimoto, E., Shiojima, I., Hiroi, Y., Zou, Y., Oka, T., Akazawa, H., Mizukami, M., Sakamoto, M., et al. (2002). Csx/Nkx2-5 is required for homeostasis and survival of cardiac myocytes in the adult heart. J. Biol. Chem. *277*, 24735–24743.

van Laake, L.W., Passier, R., Doevendans, P.A., and Mummery, C.L. (2008). Human embryonic stem cell-derived cardiomyocytes and cardiac repair in rodents. Circ. Res. *102*, 1008–1010.

Wang, L., Ma, W., Markovich, R., Chen, J.W., and Wang, P.H. (1998). Regulation of cardiomyocyte apoptotic signaling by insulin-like growth factor I. Circ. Res. *83*, 516–522.

Wilber, A., Linehan, J.L., Tian, X., Woll, P.S., Morris, J.K., Belur, L.R., McIvor, R.S., and Kaufman, D.S. (2007). Efficient and stable transgene expression in human embryonic stem cells using transposon-mediated gene transfer. Stem Cells *25*, 2919–2927.

Woll, P.S., Morris, J.K., Painschab, M.S., Marcus, R.K., Kohn, A.D., Biechele, T.L., Moon, R.T., and Kaufman, D.S. (2008). Wnt signaling promotes hematoendothelial cell development from human embryonic stem cells. Blood *111*, 122–131.

Xiong, Q., Ye, L., Zhang, P., Lepley, M., Swingen, C., Zhang, L., Kaufman, D.S., and Zhang, J. (2012). Bioenergetic and functional consequences of cellular therapy: activation of endogenous cardiovascular progenitor cells. Circ. Res. *111*, 455–468.

Xiong, Q., Ye, L., Zhang, P., Lepley, M., Tian, J., Li, J., Zhang, L., Swingen, C., Vaughan, J.T., Kaufman, D.S., and Zhang, J. (2013). Functional consequences

of human induced pluripotent stem cell therapy: myocardial ATP turnover rate in the in vivo swine heart with postinfarction remodeling. Circulation *127*, 997–1008.

Xu, C., Police, S., Hassanipour, M., and Gold, J.D. (2006). Cardiac bodies: a novel culture method for enrichment of cardiomyocytes derived from human embryonic stem cells. Stem Cells Dev. *15*, 631–639.

Zeng, L., Hu, Q., Wang, X., Mansoor, A., Lee, J., Feygin, J., Zhang, G., Suntharalingam, P., Boozer, S., Mhashilkar, A., et al. (2007). Bioenergetic and functional consequences of bone marrow-derived multipotent progenitor cell transplantation in hearts with postinfarction left ventricular remodeling. Circulation *115*, 1866–1875.

Zhang, J., Klos, M., Wilson, G.F., Herman, A.M., Lian, X., Raval, K.K., Barron, M.R., Hou, L., Soerens, A.G., Yu, J., et al. (2012). Extracellular matrix promotes highly efficient cardiac differentiation of human pluripotent stem cells: the matrix sandwich method. Circ. Res. *111*, 1125–1136.